Annals of Nuclear Energy 133 (2019) 425–430

Contents lists available at ScienceDirect

Annals of Nuclear Energy

journal homepage: www.elsevier.com/locate/anucene

# Toward a better thermal scattering law of $(C_5O_2H_8)_n$: Inelastic neutron scattering and oClimax + NJOY2016

Kemal Ramić [a,*], Carl Wendorff [a], Yongqiang Cheng [b], Alexander I. Kolesnikov [b], Doug L. Abernathy [b], Luke Daemen [b], Goran Arbanas [b], Luiz Leal [c], Yaron Danon [a], Li (Emily) Liu [a]

[a] Rensselaer Polytechnic Institute, 110 8th St, Troy, NY, USA
[b] Neutron Scattering Division, Oak Ridge National Laboratory, Oak Ridge, TN, USA
[c] Institut de Radioprotection et de Sûreté Nucléaire (IRSN), Paris, France

ARTICLE INFO

*Article history:*
Received 13 February 2019
Received in revised form 24 April 2019
Accepted 21 May 2019
Available online 6 June 2019

*Keywords:*
Phonon spectrum
ENDF
Neutron scattering
Double differential scattering cross section
GDOS
Polyethylene
Lucite
Criticality safety
Density function theory
oClimax
VISION spectrometer
ARCS spectrometer
Specific heat capacity
Thermal conductivity

ABSTRACT

With the advancements in technology (both experimental and computational) the determination of the"true" experimental phonon spectrum became more accessible. In this work a methodology for producing thermal scattering libraries from the experimental data (namely the DFT + oClimax method) for lucite $(C_5O_2H_8)_n$ is discussed. Double differential scattering cross section (DDSCS) experiments were performed at the Spallation Neutron Source of Oak Ridge National Laboratory (SNS ORNL). New scattering kernel evaluations, based on the phonon spectrum for $(C_5O_2H_8)_n$,were created using oClimax and NJOY2016 codes. In order to compare and asses the performance of the newly created library, the experimental setup was simulated using MCNP6.1. Compared to the current ENDF/B-VIII.0, the resulting RPI $(C_5O_2H_8)_n$ library improved the calculation of both double differential scattering and total scattering cross sections. A set of criticality benchmarks containing $(C_5O_2H_8)_n$ from HEU-MET-THERM resulted in an overall improved calculation of $K_{eff}$. The DFT + oClimax method is shown to be the most comprehensive method for analysis of moderator materials, due to the fact that it can be verified against all data measured at VISION, ARCS and SEQUOIA neutron spectrometers at SNS ORNL, and experimental total scattering cross section measurements. This method also provides a new technique for calculating any phonon spectrum-related quantities such as scattering law kernel, specific heat capacity, thermal conductivity, etc. for any solid state material.



## 1. Introduction

Historically the thermal scattering law (TSL) libraries, as part of Evaluated Nuclear Data Files (for example ENDF/B-VII.1) Chadwick et al. (2011), have been generated either from theoretically computed phonon spectrums (GDOS, generalized density of states), or using the phonon spectrum derived from molecular dynamics (MD) or density functional theory (DFT) calculations. An example of a library computed from a theoretical phonon spectrum would be the polyethylene TSL library, ENDF/B-VII.1, created by Koppel, Houston and Sprevak in 1969 and converted to ENDF 6 format in 1989 at Los Alamos National Lab. More recently, some of the libraries produced using MD calculations have been created by Hawari (2014). Polyethylene and lucite libraries, created by the North Caroline State University (NSCU) group, have been added to ENDF as ENDF/B-VIII.0 libraries. Furthermore, our Nuclear Data Group at Rensselaer Polytechnic Institute (RPI), has developed a new methodology for creation of TSL libraries Ramić et al. (2018). The newly developed method integrates experimentally measured data at VISION (Seeger et al., 2009), ARCS (Abernathy et al., 2012), and SEQUOIA (Granroth et al., 2010) spectrometers, at Spallation Neutron Source (SNS) at Oak Ridge National Lab (ORNL), with the density functional theory (DFT) calculations in such way that the measured experimental data are used for guiding and validation of newly created TSL libraries. The foundation for the method created by our group has been presented by Barrera et al. (2006), where the ab initio DFT modeling of polyethylene has been studied with additional analysis of the orientational effects in inelastic neutron scattering (INS) techniques. This method results in a "true" experimental neutron weighted phonon spectrum derived from DFT.

* Corresponding author.
*E-mail address:* ramick2@rpi.edu (K. Ramić).

https://doi.org/10.1016/j.anucene.2019.05.042
0306-4549/

## 2. Thermal neutron scattering theory

The Double differential scattering cross section (DDSCS) is the quantity measured at direct and indirect geometry neutron spectrometers. DDSCS represents the number of neutrons scattering into a solid angle $d\Omega$ at energy transfer increment $d\hbar\omega$ and is represented as:

$$\frac{d^2\sigma}{d\Omega d\hbar\omega} = \frac{1}{4\pi}\frac{\mathbf{k}\prime}{\mathbf{k}} S(Q,\omega), \tag{1}$$

where $\mathbf{k}\prime$ and $\mathbf{k}$ are wavevectors of final and initial neutron states respectively, $\hbar Q$ is the momentum transfer, and $S(Q,\omega)$ is the scattering law.

The proposed methodology for generation of TSL in Ramić et al. (2018) relies on two separate codes to calculate $S(Q,\omega)$: oClimax and NJOY2016. The theoretical considerations behind both codes can be seen in Ramić et al. (2018), MacFarlane and Kahler (2010), and Ramirez-Cuesta (2004); while the proposed methodology can be also seen in Ramić et al. (2018) and Ramić (2018). oClimax is a vibrational spectroscopy code that calculates the dynamic structure factor directly from the phonon information obtained from DFT codes such as CASTEP, VASP, etc.

In the proposed methodology the transformation between $S(Q,\omega)$ and GDOS is as follows, as found in Squires(Squires, 2012):

$$S_{inc\pm1}(Q,\omega) = \frac{\hbar^2Q^2}{6M\hbar\omega} exp\left(-\langle u^2\rangle Q^2\right) G(\omega)\left[n(\omega,T)+\frac{1}{2}\pm\frac{1}{2}\right] \tag{2}$$

$$n(\omega,T) = \frac{1}{exp\left(\frac{\hbar\omega}{kT}\right)-1}, \tag{3}$$

where $G(\omega)$ is GDOS (generalized density of states is DOS, density of states, weighted by squared atomic eigenvectors of vibrational modes), $\omega$ is used as frequency (1/time), and it appears with $\hbar$ (as energy in units of meV), $M$ is the atomic mass (for mono-atomic material) of the scattering material, $n(\omega,T)$ is the population Bose factor, $\langle u^2\rangle$ is the atomic mean-square displacement (MSD), and + or − are for neutrons scattered with energy loss or energy gain, respectively. The value for the MSD was chosen to be the experimental value for the material in question. In case the experimental MSD does not result in a phonon spectrum that leads to accurate total cross section when processed with NJOY2016, it was decided to vary MSD until the best agreement is obtained between the experimental and NJOY2016 calculated total cross section. With the previous methodology, this in some cases has led to exaggerating the area under the peaks at higher energy transfers, i.e., >300 meV, which is not completely physically accurate. In the mean time, oClimax has included a capability to calculate the phonon spectrum from a velocity autocorrelation function obtained from the DFT calculation. The formalism is:

$$\rho(\omega) = \frac{1}{3NTk_B}\int\sum_i \langle \mathbf{v}_i(t)\cdot\mathbf{v}_i(0)\rangle exp(i\omega t)dt, \tag{4}$$

where $\rho(\omega)$ is the energy dependent phonon spectrum, $N$ is the number of atoms in the sample material, and $\langle \mathbf{v}_i(t)\cdot\mathbf{v}_i(0)\rangle$ is the velocity autocorrelation function. The partial (atomic) density of states can be also obtained from oClimax, with a transformation from already calculated partial incoherent $S(Q,\omega)$:

$$S_{inc\pm1}(Q,\omega) = \sum_d \frac{\sigma_d}{6m_d} Q^2 exp(-2W_d)\frac{\rho_d(\omega)}{\omega}\left(n+\frac{1}{2}\pm\frac{1}{2}\right), \tag{5}$$

$$W_d = \frac{1}{6}Q^2u_d^2 \qquad n = \frac{1}{exp\left(\frac{\hbar\omega}{k_BT}\right)-1}, \tag{6}$$

where the subscript $d$ denotes the atomic species, $W_d$ is the Debye-Waller factor, and $\sigma_d$ represents bound scattering cross section.

## 3. Measurements and analysis

Similar to the measurements performed on polyethylene in Ramić et al. (2018), the DDSCS data for $(C_5O_2H_8)_n$ were measured at ARCS, which is a time-of-flight direct geometry spectrometer, and VISION, which is an indirect geometry spectrometer. The collected INS data were transformed from the time-of-flight and instrument coordinates to the dynamic structure factor $S(Q,\omega)$, corrected for the detector's efficiency. Background spectra from an empty container measured under similar conditions were subtracted from the sample data. Neutron incident energies that were used for the measurements at 5 K at ARCS were 50, 100, 250 and 700 meV. For the VISION instrument, unlike ARCS and SEQUOIA, which have fixed incident energy, the incident neutron beam is a white beam with range of incident energies, from 2 to ≈1000 meV, while the final energy is set to a fixed low energy (32 $cm^{-1}$ or 0.004 eV).

The DFT calculations for $(C_5O_2H_8)_n$ have been performed using CASTEP and the output files have been processed with oClimax to calculate $S(Q,\omega)$ for comparison with $S(Q,\omega)$ measured at VISION spectrometer. The detailed information on the CASTEP calculation can be found in Ramić (2018). The comparison can be seen in the Fig. 1.

From Fig. 1 it can be observed that the oClimax calculates the shape of the spectra reasonably well, but the locations of the peaks are off, except in the region above 300 meV. The differences in the locations of the peaks are mostly due to the structural differences in how lucite was simulated in DFT versus the lucite used for the experimental measurements, while the possible mismatch in intensities of the peaks could be due to the fact that oCLimax does not include multiple neutron scattering effects. Lucite in DFT was simulated as a crystal while the real structure of lucite is far from crystalline (lucite is a polymer, and due to the presence of methyl groups the polymer chains are prevented from packing closely in crystalline fashion or from rotating freely around the carbon–carbon bonds). It is important to note that $n$ in $(C_5O_2H_8)_n$ is part of the nomenclature and is different from n = 10 which stands for the phonon expansion order (number of multiple phonon scattering events). As introduced in Ramić et al. (2018), the frequencies of DFT output (locations of the peaks) can be scaled to match the location of the peaks in the experimental data. The comparison of scaled $S(Q,\omega)$ to the experimentally measured $S(Q,\omega)$ can be seen in Fig. 2.

After the scaling of frequencies, from Fig. 2 it can be observed that the agreement between oClimax and VISION measured S

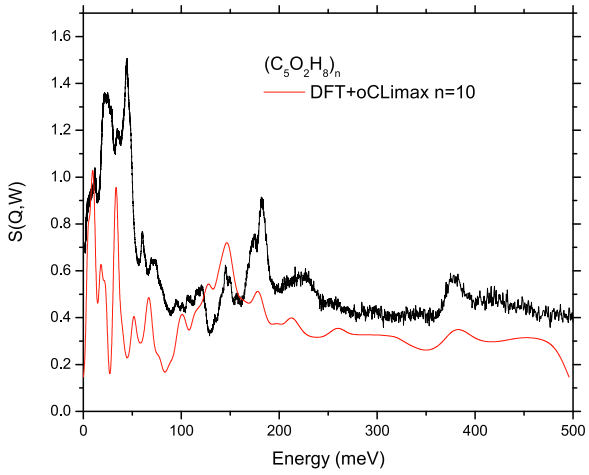


**Fig. 1.** The resulting $(C_5O_2H_8)_n$ $S(Q,\omega)$ measured at VISION spectrometer and calculated using DFT + oClimax.

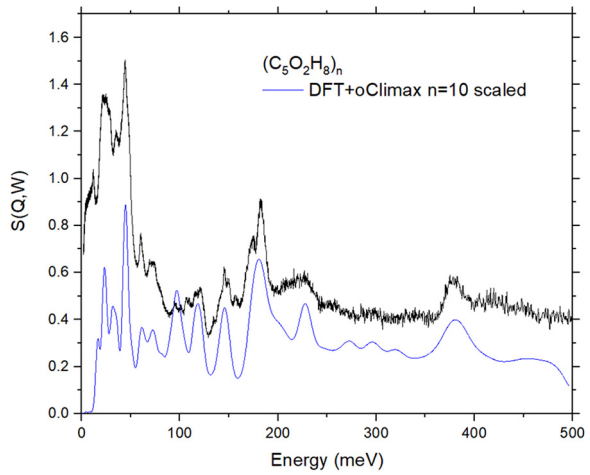


**Fig. 2.** The comparison between experimentally measured S(Q,$\omega$) for $(C_5O_2H_8)_n$ at VISION spectrometer, where the elastic line (n = 0 event) has been removed from the spectra, and the oClimax calculated S(Q,$\omega$) at 5 K temperature, where the frequencies have been scaled to match the experimental locations of the peaks.

(Q,$\omega$) has been improved significantly. Fig. 2 shows that the shape of the calculated spectrum follows the trends of the experimental data. The observed differences between calculated and experimental spectra are, similar to Fig. 1, due to multiple neutron scattering. The thickness of the lucite sample was 1.524 mm, for which transmission was 90% at 50 meV for ARCS.

For a creation of a new TSL library, NJOY2016 requires n = 1 (fundamental mode) GDOS. oClimax is capable of calculating S (Q,$\omega$) resulting from n = 1 events, as well as for multiple-phonon (n = 10) neutron scattering processes, which are compared with the VISION spectrum in Fig. 3.

Fig. 3 shows that the n > 1 events contribute to the amplitudes of the already existing peaks, while at the same time they are responsible for creation of the peaks around 300 meV that are not present at all in n = 1 calculated S(Q,$\omega$).

Using DFT and oClimax partial contributions of hydrogen, carbon and oxygen were calculated, and the resulting GDOS contributions can be seen in the Fig. 4. The comparison of the phonon spectrum for hydrogen in $(C_5O_2H_8)_n$ generated directly with the oClimax and the one obtained using the previous developed

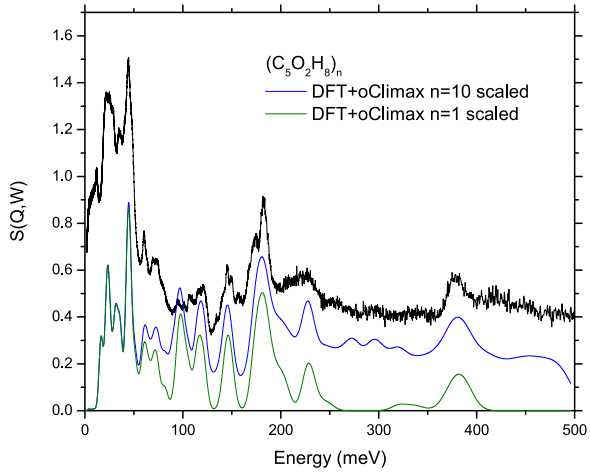


**Fig. 3.** The comparison between experimentally measured S(Q,$\omega$) for $(C_5O_2H_8)_n$ at VISION spectrometer, where the elastic line (n = 0 event) has been removed from the spectra, the scaled oClimax calculated S(Q,$\omega$) resulting from n = 10 events, and the scaled oClimax calculated S(Q,$\omega$) resulting from the fundamental mode (n = 1 quantum event) at 5 K temperature.

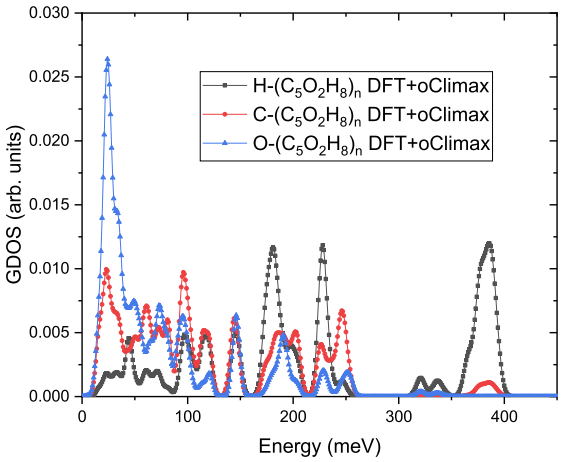


**Fig. 4.** The comparison between hydrogen, carbon and oxygen contribution to $(C_5O_2H_8)_n$ GDOS.

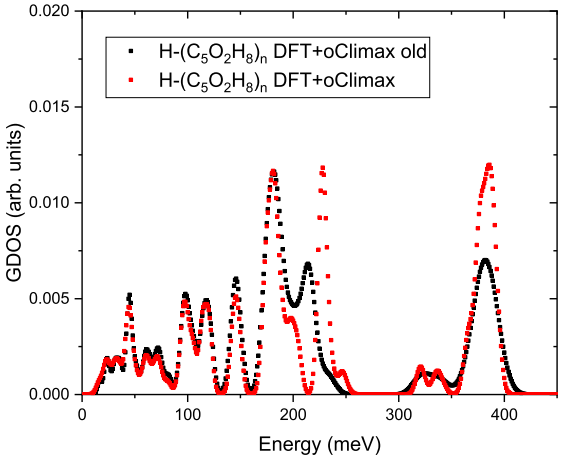


**Fig. 5.** The comparison between H-$(C_5O_2H_8)_n$ GDOS generated directly by oClimax and one derived with the previous RPI methodology.

methodology, where the MSD is varied to match the experimental total cross section, can be seen in Fig. 5.

## 4. Library validation

The molecular dynamics-based ENDF/B-VIII.0 library, created by NCSU Nuclear Reactor Program group Hawari (2014), contains only thermal scattering library for hydrogen in $(C_5O_2H_8)_n$. The comparison between hydrogen partial GDOS used to create ENDF/B-VIII.0 library and the hydrogen GDOS derived from oClimax can be seen in the Fig. 6.

As can be seen from Fig. 6, there are slight differences in the locations of the peaks between two sets of partial GDOS. It is quite clear that those differences arise from the scaling of frequencies that was performed to get the oClimax S(Q,$\omega$) to match the experimentally measured S(Q,$\omega$) at VISION spectrometer. Also, there are slight differences in the amplitudes of the peaks.

In order to assess the performance of the new library, an analysis of how the two different libraries perform in MCNP simulation of ARCS spectrometer has been performed. The comparison between the ENDF/B-VIII.0 and the NJOY processed library produced from our DFT + oClimax is represented in Fig. 7.

It can be observed from Fig. 7 that the RPI DFT + oCLimax library performs better than the ENDF/B-VIII.0 library. The ENDF/B-VIII.0 library fails to reproduce some of the structural information

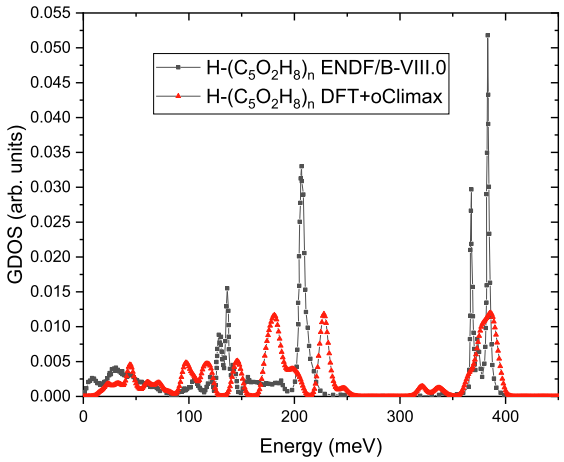


**Fig. 6.** The comparison between hydrogen partial contribution to $(C_5O_2H_8)_n$ GDOS used to create ENDF/VIII library and GDOS derived directly from oClimax.

(location of certain peaks), while DFT + oCLimax library shows all the significant structural information (especially at higher incident energy, 250 meV), although some of the peaks are exaggerated at lower incident energy. Also, at lower incident energy (i.e. 100 meV), for the RPI library the elastic peak is exaggerated. The height of the elastic peak is directly related to the Debye-Waller coefficient.

The next step in the assessment of the performance of these libraries is to check how well the total cross section is calculated. For DFT + oClimax library the total cross section has been calculated as follows (where subscripts $s$ and $\gamma$ represent the scattering and absorption cross section components, respectively):

$$\sigma_{(C_5O_2H_8)_n,t}(E) = 8 \times \left(\sigma_{H,s}^{\text{NJOY2016}}(E) + \sigma_{H,\gamma}^{\text{ENDF}}(E)\right) + 5 \times \left(\sigma_{C,s}^{\text{NJOY2016}}(E) + \sigma_{C,\gamma}^{\text{ENDF}}(E)\right) + 2 \times \left(\sigma_{O,s}^{\text{NJOY2016}}(E) + \sigma_{O,\gamma}^{\text{ENDF}}(E)\right). \quad (7)$$

Because the ENDF/B-VIII.0 library is created as H-$(C_5O_2H_8)_n$, the total cross section is calculated as follows (where subscript $t$ represents the total cross section):

$$\sigma_{(C_5O_2H_8)_n,t}(E) = 8 \times \left(\sigma_{H,s}^{\text{NJOY2016}}(E) + \sigma_{H,\gamma}^{\text{ENDF}}(E)\right) + 5 \times \left(\sigma_{C,t}^{\text{ENDF}}(E)\right) + 2 \times \left(\sigma_{O,t}^{\text{ENDF}}(E)\right). \quad (8)$$

As can be seen from Fig. 8, the RPI library performs better than the ENDF/B-VIII.0 library across the entire energy range, except in the 10 to approximately 30 meV range. Below 10 meV both libraries deviate from the experimental data, but the RPI library follows the trend of the experimental data, although it is under calculating, while the ENDF/B-VIII.0 library calculates the total cross section more as a straight line.

The final test of the new libraries is to perform critical benchmarks on them to see if there is a significant impact on the effective multiplication factor ($K_{eff}$) calculation. The critical benchmarks, that contain $(C_5O_2H_8)_n$, were chosen using the Database for the International Handbook of Evaluated Criticality Safety Benchmark Experiments (DICE) (DICE, 2017). More details on the benchmarks chosen and how the calculations were performed can be found in Wendorff et al. (2019). The results for $(C_5O_2H_8)_n$ can be seen in Fig. 9 and Table 1. The standard deviation is only reported for the experimental data.

It can be observed from the Fig. 9 that the simulations without a scattering kernel (free gas model) result in overestimating the $K_{eff}$,

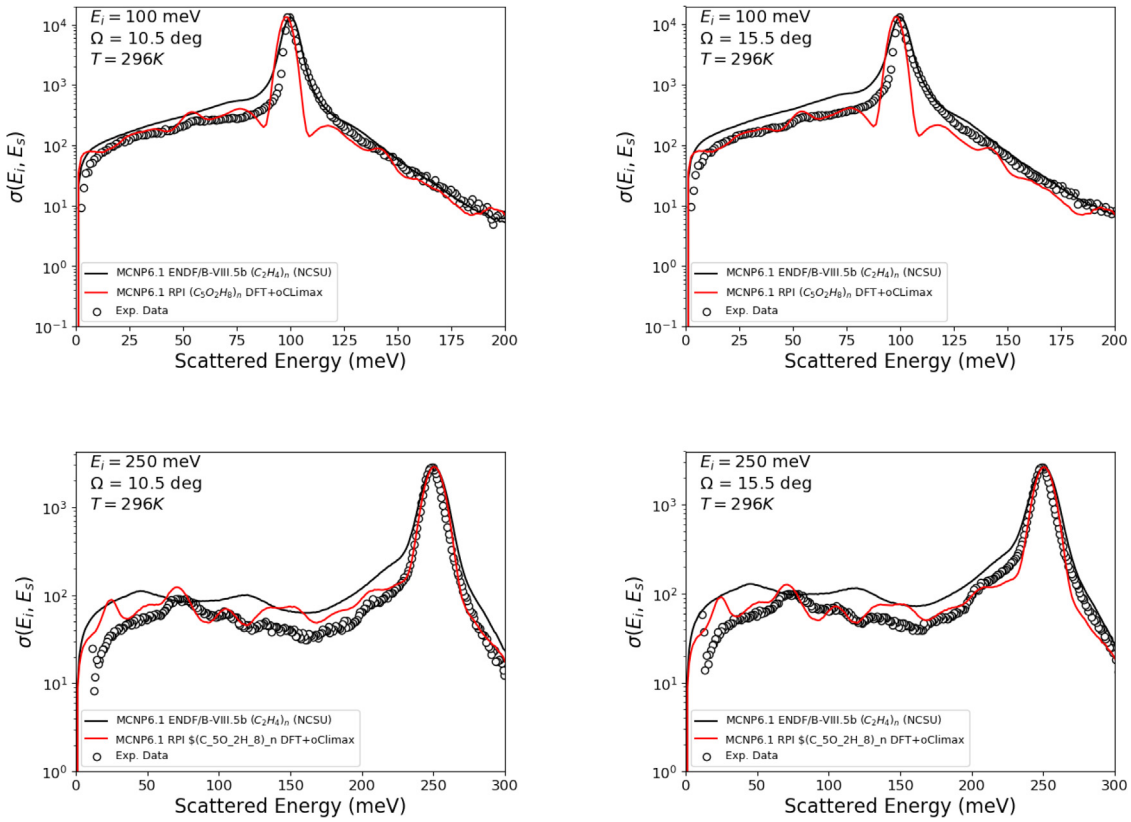


**Fig. 7.** DDSCS comparison at the 100 and 250 meV incident energies, at scattering angles 10.5 and 15.5°.

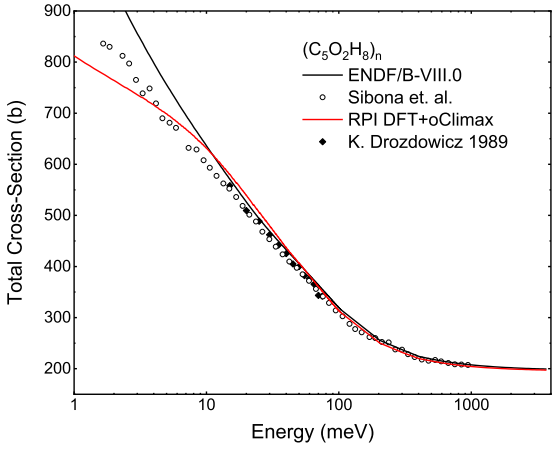


**Fig. 8.** Total cross section of $(C_5O_2H_8)_n$.

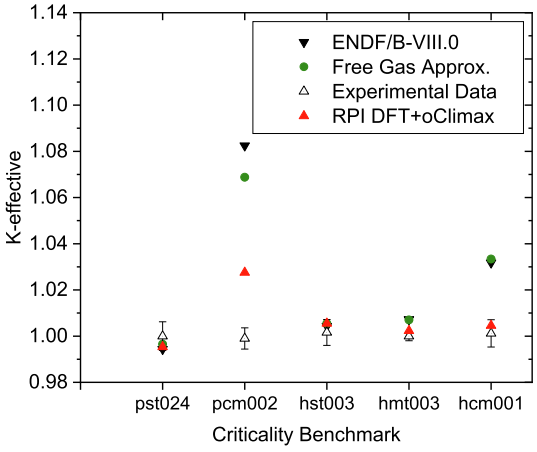


**Fig. 9.** $K_{eff}$ comparison for $(C_5O_2H_8)_n$ critical benchmarks. Each x-axis point represents a different $(C_5O_2H_8)_n$ moderated critical benchmark. The uncertainty is only from the experimental benchmark.

**Table 1**
$K_{eff}$ comparison for $(C_5O_2H_8)_n$ critical benchmarks.

| Critical Benchmark | $(C_5O_2H_8)_n$ library | $K_{eff}$ | Std. dev. |
|---|---|---|---|
| pst024 | Experimental | 1.00 | 0.0062 |
| pst024 | ENDF/B-VIII.0 | 0.99437 | N/A |
| pst024 | RPI DFT + oClimax | 0.99533 | N/A |
| pst024 | Free Gas Approx. | 0.99651 | N/A |
| pcm002 | Experimental | 0.999 | 0.0046 |
| pcm002 | ENDF/B-VIII.0 | 1.08246 | N/A |
| pcm002 | RPI DFT + oClimax | 1.02756 | N/A |
| pcm002 | Free Gas Approx. | 1.06877 | N/A |
| hst003 | Experimental | 1.0016 | 0.0056 |
| hst003 | ENDF/B-VIII.0 | 1.00429 | N/A |
| hst003 | RPI DFT + oClimax | 1.00552 | N/A |
| hst003 | Free Gas Approx. | 1.00552 | N/A |
| hmt003 | Experimental | 1.00 | 0.002 |
| hmt003 | ENDF/B-VIII.0 | 1.00723 | N/A |
| hmt003 | RPI DFT + oClimax | 1.00232 | N/A |
| hmt003 | Free Gas Approx. | 1.00701 | N/A |
| hcm001 | Experimental | 1.0012 | 0.0059 |
| hcm001 | ENDF/B-VIII.0 | 1.03179 | N/A |
| hcm001 | RPI DFT + oClimax | 1.00458 | N/A |
| hcm001 | Free Gas Approx. | 1.03335 | N/A |

while the ENDF/B-VIII.0 library performed similarly or worse than the free gas model. The RPI DFT + oClimax library consistently performed better than ENDF/B-VIII.0 library. The improved performance of the library is due to the fact that the total cross section changed, systematically lowering down the calculated $K_{eff}$ values. It is important to note that before the RPI lucite library it was thought that the benchmarks were not sensitive to lucite, which has been proven wrong.

## 5. Conclusion and future work

A thorough analysis of the experimental data with a combination of DFT and oClimax has led to an improved $(C_5O_2H_8)_n$ library, with improvements noticeable in double differential and total cross sections calculations, while the benchmarks also show significant improvement in $K_{eff}$ calculation.

The DFT + oClimax method has been shown to be the most complete method for obtaining "true" experimental phonon spectrum. The importance of the DFT + oClimax method created scattering kernels is in the fact that they can be verified against all data measured at VISION, ARCS and SEQUOIA, and experimental total scattering cross section measurements, while providing a new technique for calculating any phonon spectrum related quantities such as scattering law kernel, specific heat capacity, thermal conductivity, etc.

## Acknowledgements

This research was supported by the Nuclear Criticality Safety Program in the U.S. Department of Energy

This research used resources of the National Energy Research Scientific Computing Center, a DOE Office of Science User Facility supported by the Office of Science of the U.S. Department of Energy.

The research at Oak Ridge National Laboratory's Spallation Neutron Source was sponsored by the U.S. Department of Energy and by the Scientific User Facilities Division, Office of Basic Energy Sciences, the U.S. Department of Energy.

## Appendix A. Supplementary data

Supplementary data associated with this article can be found, in the online version, at https://doi.org/10.1016/j.anucene.2019.05.042.

## References

Abernathy, D.L., Stone, M.B., Loguillo, M.J., Lucas, M.S., Delaire, O., Tang, X., Lin, J.Y.Y., Fultz, B., 2012. Design and operation of the wide angular-range chopper spectrometer ARCS at the Spallation Neutron Source. Rev. Scientific Instrum. 83. https://doi.org/10.1063/1.3680104.

Barrera, G.D., Parker, S.F., Ramirez-Cuesta, A.J., Mitchell, P.C.H., 2006. The vibrational spectrum and ultimate modulus of polyethylene. Macromolecules 39, 2683–2690. https://doi.org/10.1021/ma052602e.

Chadwick, M., Herman, M., Obložinský, P., Dunn, M., Danon, Y., Kahler, A., Smith, D., Pritychenko, B., Arbanas, G., Arcilla, R., Brewer, R., Brown, D., Capote, R., Carlson, A., Cho, Y., Derrien, H., Guber, K., Hale, G., Hoblit, S., Holloway, S., Johnson, T., Kawano, T., Kiedrowski, B., Kim, H., Kunieda, S., Larson, N., Leal, Lestone, J., Little, R., McCutchan, E., MacFarlane, R., MacInnes, Mattoon, C., McKnight, R., Mughabghab, S., Nobre, G., Palmiotti, G., Palumbo, A., Pigni, M., Pronyaev, V., Sayer, R., Sonzogni, A., Summers, N., Talou, P., Thompson, I., Trkov, A., Vogt, R., van der Marck, S., Wallner, A., White, M., Wiarda, D., Young, P., 2011. ENDF/B-VII.1 nuclear data for science and technology: cross sections, covariances, fission product yields and decay data. Nucl. Data Sheets 112, 2887–2996.

Database for the international criticality safety benchmark evaluation project (dice).http://icsbep.inel.gov/ (accessed 05.03.2017)..

Granroth, G., Kolesnikov, A., Sherline, T., Clancy, J., Ross, K., Ruff, J., Gaulin, B., Nagler, S., 2010. SEQUOIA: a newly operating chopper spectrometer at the SNS. J. Phys.: Conf. Ser. 251, 012058.

Hawari, A., 2014. Modern techniques for inelastic thermal neutron scattering analysis. Nucl. Data Sheets 118, 172–175.

MacFarlane, R., Kahler, A., 2010. Methods for processing ENDF/B-VII with NJOY. Nucl. Data Sheets 111, 2739–2890.
Ramić, K., 2018. From Experiments to DFT Simulations: Comprehensive Overview of Thermal Scattering For Neutron Moderator Materials (PhD dissertation). Rensselaer Polytechnic Institute.
Ramić, K., Wendorff, C., Cheng, Y., Kolesnikov, A.I., Abernathy, D.L., Daemen, L., Arbanas, G., Leal, L., Danon, Y., Liu, L.E., 2018. Thermal scattering law of (C2H4) n: integrating experimental data with DFT calculations. Ann. Nucl. Energy 120, 778–787.
Ramirez-Cuesta, A., 2004. aCLIMAX 4.0.1, the new version of the software for analyzing and interpreting INS spectra. Comput. Phys. Commun. 157, 226–238.
Seeger, P.A., Daemen, L.L., Larese, J.Z., 2009. Resolution of VISION, a crystal-analyzer spectrometer. Nucl. Instrum. Methods Phys. Res. Sect. A 604, 719–728.
Squires, G.L., 2012. Introduction to the Theory of Thermal Neutron Scattering. Cambridge University Press.
Wendorff, C., Ramic, K., Liu, L., Danon, Y., Kolesnikov, A.I., Abernathy, D., 2019. Improved experimental data for accurate thermal scattering kernel evaluations of water, polyethylene, and quartz..